ACS Photonics

Article

pubs.acs.org/journal/apchd5

High Efficiency Tandem Organic Light Emitting Diode Using an Organic Heterojunction as the Charge Generation Layer: An Investigation into the Charge Generation Model and Device Performance

Hengda Sun,[†] Qingxun Guo,[†] Dezhi Yang,[†] Yonghua Chen,[‡] Jiangshan Chen,[†] and Dongge Ma*[,†]

[†]State Key Laboratory of Polymer Physics and Chemistry, Changchun Institute of Applied Chemistry, University of Chinese Academy of Sciences, Changchun 130022, People's Republic of China

[‡]Center of Advanced Science and Engineering for Carbon (Case4Carbon), Department of Macromolecular Science and Engineering, Case School of Engineering, Case Western Reserve University, 10900 Euclid Avenue, Cleveland, Ohio 44106, United States

ABSTRACT: Organic heterojunctions (OHJs) are frequently used as charge generation layers (CGLs) in the construction of high efficiency tandem organic light emitting diodes (OLEDs). However, the charge generation mechanism still remains unclear. In this article, the working principle of a typical OHJ CGL composed of 1,4,5,8,9,12-hexaazatriphenylene-hexacarbonitrile (HAT-CN)/4,4′,4″-tris(N-3-methylphenyl-*N*-phenylamino)triphenylamine (m-MTDATA) is studied. We found that the charge generation process in this OHJ results from electron tunneling, which is shown through temperature-dependent *J*−*V* characteristics and model fitting. Additionally, we fabricated an ultrahigh efficiency green tandem OLED using only commercially available organic semiconductor materials for OLED. The maximum power efficiency reaches 120 lm/W, yet remains at 110.3 lm/W at 1000 cd/m^2, which is greatly enhanced from when compared to the corresponding single-unit device. The maximum current efficiency and external quantum efficiency reach as high as 201 cd/A and 54.5%, respectively.

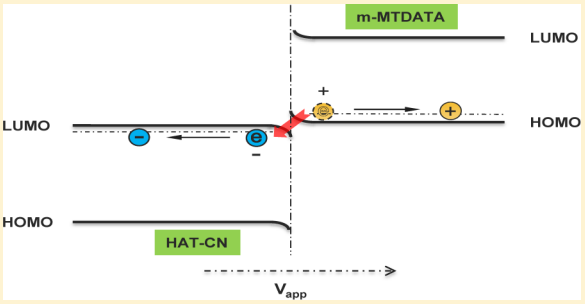

KEYWORDS: *organic light-emitting diodes, charge generation layers, organic heterojunctions, charge tunneling*

Organic light emitting diodes (OLEDs) are regarded as the most promising candidate for next generation displays and lighting because of the advantages resulting from surface emitting, the ease of manufacturing large areas, the possibility for flexible and transparent applications, and the vast number of available materials for specific demands.[1−4] In the past decade, a substantial effort has been undertaken to improve both the efficiency and lifetime of OLEDs to satisfy the requirements of mass production.[3,5−11] Tandem (or stacked) OLEDs are promising devices that can potentially achieve both a high efficiency and long operating time.[12−15] A typical tandem OLED is fabricated by vertically connecting several individual electroluminescent (EL) units in series via the charge generation layer (CGL); the entire device is driven by a single power source.[16−18] When a certain voltage is applied on the electrodes, each EL lights up individually under the identical current that flows through the entire device. In fact, an OLED is a current driven device; with increasing current density, the luminance of the device increases whereas the operational lifetime decreases.[1,19,20] Because tandem OLEDs can obtain the identical brightness under several folds of lower current density (depending on the number of EL units), the lifetime of the OLED can be significantly lengthened. Furthermore, the tandem structure provides the feasibility that EL units of different colors can be vertically stacked for color tuning and white light emission.[12,14,16,21]

As the most important part in a tandem OLED, the charge generation layer (CGL) can be formed by using a metal−metal (or metal oxide) bilayer, organic−metal (or metal oxide) bilayer, or p-doping/n-doping organic bilayer.[18] However, those CGLs suffer from certain problems that potentially limit their wide application. For example, some metal oxides commonly used in CGLs and p-doping form complexes with the migrated n-dopants from the adjacent electron transporting layer when operating, which would result in significant performance degradation and driving a voltage increase.[13,22] In fact, the increase in the operational voltage with the increase in the number of EL units is a common problem in tandem OLEDs. As a result, the power efficiency of the fabricated tandem OLED is inferior to that of the best performing single-unit OLED.[23−25] Therefore, designing new CGLs to reduce the operational voltage and enhance the power efficiency of tandem OLEDs has become the latest points of research interest. Recently, OHJs composed of a p-type organic semiconductor and an n-type organic semiconductor can be considered as

Received: October 6, 2014
Published: January 15, 2015

DOI: 10.1021/acsphotonics.5b00010
ACS Photonics 2015, 2, 271−279

effective CGLs that show a great stability and high efficiency.[13−15,17,26−31] However, some of these OHJs are introduced from organic solar cells, such as phthalocyanine complexes and fullerene. One inevitable problem for these photovoltaic materials is that they possess optical absorptions in the visible spectral regions, resulting in some optical losses within the CGLs.[30,32,33] In addition, the solar cell materials are generally more difficult to match to the energy levels of commonly used OLED materials, leading to interface barriers between CGLs and charge transport layers. In this case, some interfacial modification layers have to be introduced to reduce the interface barriers, complicating the device structure.[14,15,29,30] Most importantly, the majority of the studies in the field of tandem OLEDs concentrate on device performance; no proper theoretical model has been developed to explain the charge generation process of organic OHJs as CGLs, which is important in the design of high efficiency tandem OLEDs.

In this paper, we present a simple and effective organic OHJ CGL composed of a p-type organic material, 4,4′,4″-tris(N-3-methylphenyl-*N*-phenylamino)triphenylamine (m-MTDATA), and an n-type organic material, 1,4,5,8,9,12-hexaazatriphenylene-hexacarbonitrile (HAT-CN). With the bilayer structure of this CGL, we fabricated an ultrahigh efficiency tandem OLED based only on commonly used commercial organic semiconductor materials. The maximum power efficiency can reach 120 lm/W and remain at 110.3 lm/W at 1000 cd/m^2, which are greatly enhanced relative to the corresponding single-unit device. The maximum current efficiency and external quantum efficiency can reach as high as 201 cd/A and 54.5%, respectively, and only decrease to 195.2 cd/A and 51.2%, respectively, at 1000 cd/m^2. These values are among the best results published. Furthermore, the working principles of the organic OHJs as CGLs are studied in detail and explained by a Zener tunneling model.

RESULTS AND DISCUSSION

When organic heterojunctions are employed as CGLs, these junctions usually contain two organic layers deposited successively to form a donor−acceptor system to promote charge generation and transfer.[13,15,28,34] HAT-CN is a strong electron acceptor with a LUMO as low as 4.8 eV.[35] Considering that the HOMO of most of the commonly used hole-transporting materials are between 5 and 6 eV, the HAT-CN is suitable to form a donor−acceptor system. To select an appropriate hole transporting material (HTM) to form an OHJ with HAT-CN, a set of devices is prepared: ITO and MoO_3 (3 nm) with 20 wt % MoO_3; TAPC (50 nm), HTM (15 nm), and HAT-CN (15 nm) with 3 wt % Cs; and BPhen (50 nm), CS (1 nm), and Al (100 nm). A comparison of the *J*−*V* properties is given in Figure 1. Some of the combinations have already been reported by other groups such as NPB/HAT-CN and TAPC/HAT-CN.[13,15] The symmetry of the *J*−*V* characteristic of CGL structures is an indicator of the efficiency of the charge generation at the interface. The charge generation increases as the *J*−*V* curve becomes more symmetrical.[36] In Figure 1, the m-MTDATA/HAT-CN OHJ has the best symmetry and the largest current density at a certain bias for all materials tested. Therefore, this OHJ should possess a better charge generation efficiency, and we select this design as our main research focus. Considering the wide optical band gaps of both materials (Table 1), the excess light absorption in the visible spectrum range in the CGL composed of m-MTDATA/HAT-CN could also be avoided when employed in tandem OLEDs.

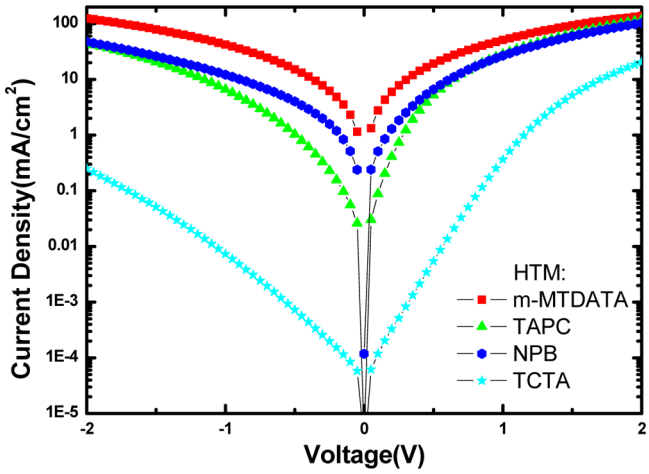

Figure 1. Comparison of the *J*−*V* properties of several OHJs: ITO/MoO_3 (3 nm) with 20 wt % MoO_3; TAPC (50 nm), HTM (15 nm), and HAT-CN (15 nm) with 3 wt % Cs; and ND BPhen (50 nm), CS (1 nm), and Al (100 nm). For the above structures, the HTM is m-MTDATA, TAPC, NPB, and TCTA, respectively.

Table 1. Energy Levels of the Materials

abbreviation	HOMO (eV)	LUMO (eV)	triplet energy (eV)	ref.
HAT-CN	9.6	4.8		35
m-MTDATA	5.1	1.9	2.58	37
TAPC	5.4	2.0	2.9	38
TCTA	5.7	2.3	2.86	23
$Ir(ppy)_2(acac)$	5.0	2.6	2.3	39
BPhen	6.4	3.0	2.5	40
MoO_3	9.7	6.7		41

To test the validity of the device as a CGL, a two-unit green phosphorescent tandem OLED connected by a m-MTDATA/HAT-CN OHJ is fabricated. Molybdenum trioxide (MoO_3) doped 4,4′-cyclohexylidenebis[*N*,*N*-bis(4-methylphenyl)-benzenamine] (TAPC) is used as the hole transporting layer, and cesium-doped bathophenanthroline (BPhen) is used as the electron transporting layer. A green phosphorescent emitter, bis(2-phenylpyridine)(acetylacetonato)iridium(III) ($Ir(ppy)_2(acac)$), is doped into tris(4-carbazoyl-9-ylphenyl)amine (TCTA) and BPhen to form the double-emitting layers (D-EMLs). Two intrinsic layers of TAPC and BPhen are placed between the EML and charge transport layer to function as the electron and hole blocking layer, respectively. These layers also serve as excitation blocking layers to confine the triplet excitations in the D-EMLs. The structure of the device is given below (Device A): ITO (170 nm) and MoO_3 (3 nm) with 25 wt % MoO_3; TAPC (50 nm) and TAPC (10 nm) with 8 wt % $Ir(ppy)_2(acac)$; TCTA (6 nm) with 8 wt % $Ir(ppy)_2(acac)$; BPhen (8 nm) and BPhen (10 nm) with 3 wt % Cs; BPhen (35 nm), HAT-CN (15 nm) and m-MTDATA (15 nm) with 25 wt % MoO_3; TAPC (35 nm) and TAPC (10 nm) with 8 wt % $Ir(ppy)_2(acac)$; TCTA (6 nm) with 8 wt % $Ir(ppy)_2(acac)$; BPhen 8% (8 nm) and BPhen (10 nm) with 3 wt % Cs; and BPhen (45 nm), Cs (1 nm), and Al (100 nm). Additionally, a single unit device is prepared for comparison (Device B): ITO (170 nm) and MoO_3 (3 nm) with 25 wt % MoO_3; TAPC (50 nm) and TAPC (10 nm) with 8 wt % $Ir(ppy)_2(acac)$; TCTA (6 nm) with 8 wt % $Ir(ppy)_2(acac)$; BPhen (8 nm) and BPhen (10 nm) with 3 wt % Cs; BPhen (45 nm), Cs (1 nm), and Al (100 nm). A

DOI: 10.1021/acsphotonics.5b00010
ACS Photonics 2015, 2, 271−279

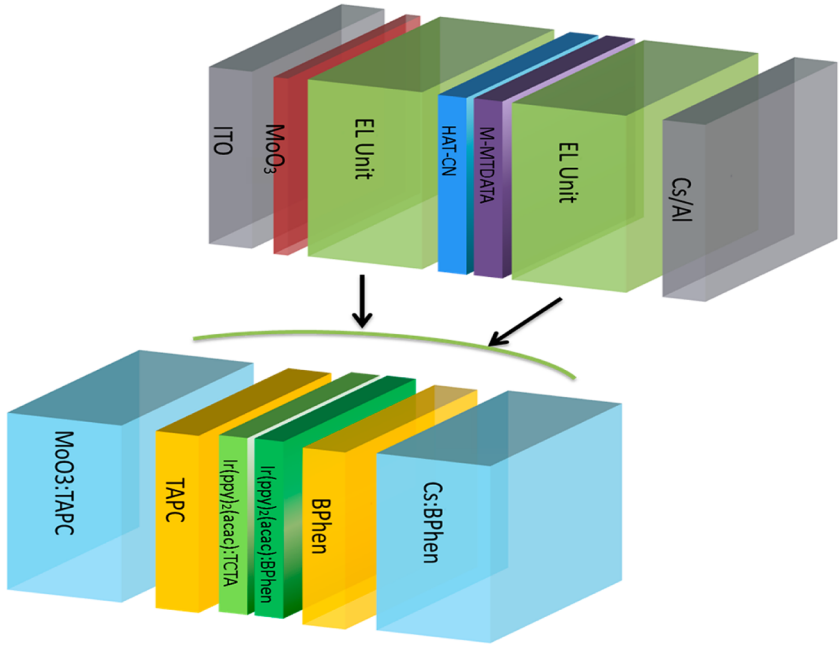

Figure 2. Schematic diagram of the tandem device structure.

schematic diagram of the tandem device structure is given in Figure 2. All energy levels of the materials used in this study are shown in Table 1. Both devices are optimized to achieve the best external quantum efficiency. As shown in Table 2, the turn-on voltage of device A is 4.9 V, which is about twice the voltage of the single device. At a higher brightness, the operating voltage of device A is two times smaller than that of device B (6.0 V vs 3.2 V @ 10000 cd/m^2). This result indicates that the m-MTDATA/HAT-CN OHJ should possess a rather high conductivity with a small voltage drop. From Figure 3 and Table 2, the current efficiency is enhanced from 80.4/81.8/72.7 (cd/A) of the single unit to 200.8/195.2/185.7 (cd/A) of the tandem OLED at 100/1000/10000 (cd/m^2), respectively. These values exceed twice the initial value. According to the definition of current efficiency, the brightness of device A is more than twice of that of device B for the identical current density. The current density−voltage-brightness characteristics are displayed in Figure 3a. Although the voltage is doubled, the brightness more than doubled, from 820 cd/m^2 for device B to 1920 cd/m^2 for device A at 1 mA/cm^2. The power efficiency is also improved, reaching 120 lm/W at the maximum and only slightly reducing to 119.4/110.3/99.7 (lm/W) at 100/1000/10000 (cd/m^2). Device A displays a low efficiency decay, higher than that of device B (Table 2). To the best of our knowledge, this result is the highest power efficiency published for tandem OLEDs without using outcoupling technology. The spectra of both devices remain almost identical (Figure 3c, inset), indicating that the microcavity effect in the tandem device is not obvious.

Theoretically, the tandem structure OLED will not improve the maximum power efficiency of a specific EL unit. When two identical EL units are used as the reference single-unit OLED and are connected by a CGL, the power efficiency of the resulting tandem OLED will remain unchanged because of the doubled operational voltage, although the resulting current efficiency could be twice that of the reference OLED. Furthermore, if the extra voltage drop across the CGL in the tandem device is considered, the actual power efficiency could be even lower than that of conventional OLEDs. Therefore, enhancing the power efficiency of tandem OLEDs requires either an increase in the brightness or a reduction in the operational voltage at a certain current density. This is the method that improved the power efficiency of the tandem OLED.

Further increases in the brightness of the tandem OLED indicates that the charge generation process in the m-MTDATA/HAT-CN CGL must be efficient, which is guaranteed by the charge tunneling nature of the device. Therefore, the charge generation process is not the rate-determining step for the current density increase. In other words, the CGL could generate enough charge to recombine with the injected charge at the emitting layers. This process reduces the accumulation of excessively injected charges which would otherwise result in excitation quenching. Therefore, the total brightness is enhanced. Additionally, the tandem OLED is thicker than traditional OLEDs. Therefore, the leakage current would be reduced, and a higher current efficiency can be expected.[24] Moreover, the two emitting layers in the tandem OLED are designed to locate the first and second antinode away from the aluminum cathode in such a way to achieve maximum brightness. As reported, the fraction of radiation coupled into the surface-plasmon modes would be less when the emitter is further away from the cathode, the maximum forward luminance occurs roughly corresponding to the antinodes of the metal electrodes because of the interaction between the microcavity and surface-plasmon modes.[42]

The further reduction of operational voltage in the tandem device could be attributed to the electrical properties of the m-MTDATA/HAT-CN CGL. Generally, the role of the CGL in tandem OLEDs includes charge carrier generation, transportation and injection. Apart from generating charges effectively, the reduction in the operational voltage requires that the CGL should be highly conductive to facilitate the transportation of the generated charges, and the injection barriers at the interfaces of the CGL and adjacent EL units should be as small as possible. Considering the energy levels of

DOI: 10.1021/acsphotonics.5b00010
ACS Photonics 2015, 2, 271−279

Table 2. Comparison of the Single Unit Device and Tandem Device

device	turn-on voltage (V)	voltage (V) @100/1000/10000 (cd/m^2)	current efficiency (cd/A) @100/1000/10000 (cd/m^2)	power efficiency (lm/W) @100/1000/10000 (cd/m^2)	external quantum efficiency (%) @100/1000/10000 (cd/m^2)
A	4.9	5.3/5.6/6.0	200.8/195.2/185.7	119.4/110.3/99.7	54.5/51.2/46.4
B	2.4	2.6/2.8/3.2	80.4/81.8/72.7	96.8/92.8/70.8	21.9/22.2/19.5

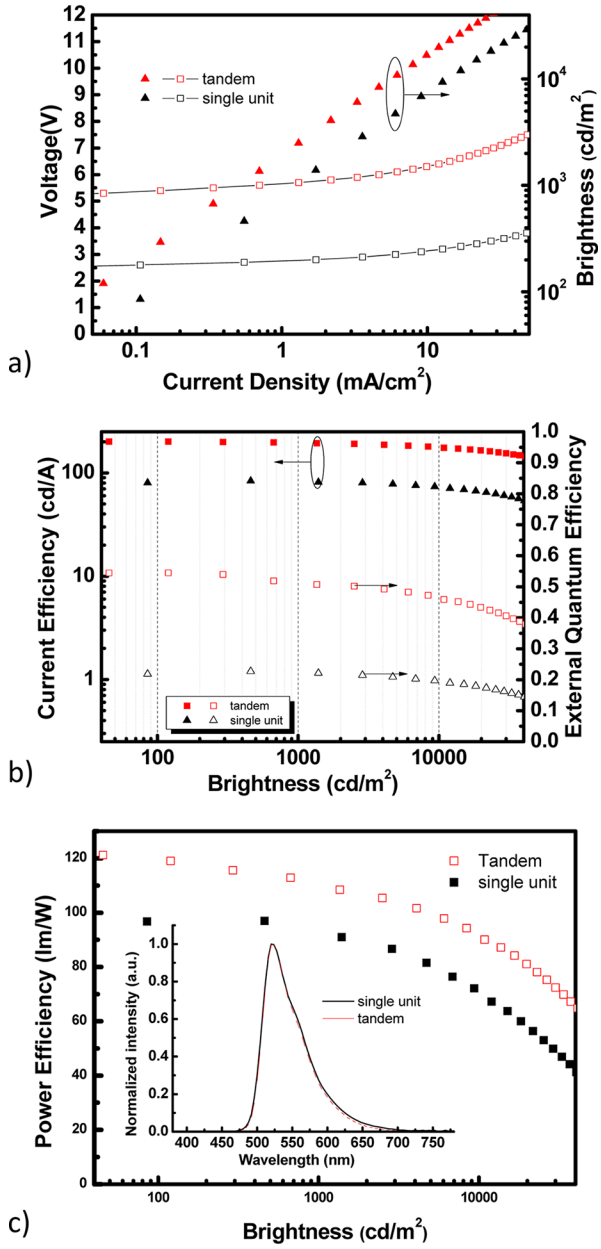

Figure 3. Comparisons of the tandem and single unit devices: (a) the current density−luminance−voltage characteristics; (b) brightness vs current efficiency and external quantum efficiency; and (c) brightness vs power efficiency. The inset displays the EL spectra of the tandem device and the single unit under the identical brightness of 1000 cd/m^2.

HAT-CN and m-MTDATA, the intrinsic Fermi level of m-MTDATA would be higher than that of HAT-CN. Therefore, when these materials contact, they would form an accumulation type OHJ according to Yan et al.[43] The accumulation type OHJ indicates that holes will accumulate at the p-side m-MTDATA and electrons will accumulate at the n-side HAT-CN, distinct from typical p−n junctions, which form charge depletion regions near the interface of the OHJ. As shown in the previous investigation, OHJs with accumulation-type space charge regions can efficiently generate charges.[28] One significant advantage of this accumulation type OHJ is that the accumulated electrons and holes can greatly increase the density of movable carriers, thus increasing the charge mobility

DOI: 10.1021/acsphotonics.5b00010
ACS Photonics 2015, 2, 271−279

by several magnitudes.[43] In this case, the bulk voltage drop across the m-MTDATA/HAT-CN OHJ caused by transporting generated electrons and holes could be reduced to a minimum. Furthermore, the HOMO of m-MTDATA is 5.1 eV, matching well with that of MoO_3: TAPC. Therefore, the injection of holes is efficient without using an extra modification layer. The injection of electrons from HAT-CN to n-doped Bphen is also an efficient process.[44] The discussion above indicates that the m-MTDATA/HAT-CN OHJ possesses all of the important features required to be an effective CGL: effective charge generation, high conductivity, and good injection properties. The high efficiencies in the tandem OLED support this point.

To elucidate the mechanism of charge generation in the m-MTDATA/HAT-CN CGL, we fabricated the following device: ITO and MoO_3 (3 nm) with 20 wt % MoO_3; TAPC (50 nm), m-MTDATA (15 nm), and HAT-CN (15 nm) with 3 wt % Cs; and BPhen (50 nm), Cs (1 nm), and Al (100 nm; device C). The p-doping/OHJ/n-doping structure is introduced to simulate the sequences in a real tandem device (when device A is under a reverse bias, the current flows like the tandem device we fabricated above) and to ensure ohmic contact at the electrodes.[24,45] Considering the high conductivity of the MoO_3/TAPC and Cs/BPhen doping layers, the voltages would mainly drop on the m-MTDATA/HAT-CN heterojunction.[40] Therefore, the $J-V$ characteristics of the device will be determined by the electrical properties of the heterojunction. When under a forward bias, holes and electrons are injected from the electrodes and are recombined at the interface of the OHJ. When under a reverse bias, the current is mainly generated by the CGL rather than being injected. Because we doped the hole and electron transporting layers beside the electrodes, the injection of opposite charge carriers should be difficult. To further confirm these properties, a device with only m-MADATA between the charge transport layers is prepared: ITO and MoO_3 (3 nm) with 20 wt % MoO_3; TAPC (50 nm) and m-MADATA (15 nm) with 3 wt % Cs; and BPhen (50 nm), CS (1 nm), and Al (100 nm; device D). Because of the lack of accumulating OHJ for charge generation, the reverse current of device D would be determined by the charge injected from the electrodes. Figure 5 compares the current density−voltage characteristics of devices C and D. The reverse current density of device D is approximately five magnitudes lower than that of device C, which indicates that the charges injected from the electrodes under reverse bias is small when compared to the generated current and can be ignored.

An additional process also explains the charge generation process by using capacitance−voltage measurements, which has been illustrated in previous studies.[30,31,46,47] The device is similar to devices C and D, but another 100 nm of LiF is added beside both electrodes to serve as an insulation layer and to prohibit charge injection. In Figure 4, the two devices exhibit rather different $C-V$ behaviors; the capacitance of the device with only m-MTDATA remains almost unchanged throughout the entire bias range from 0 to 8 V, whereas the device with the HAT-CN/m-MTDATA OHJ shows an increasing trend of capacitance even at a relatively low voltage. These results indicate that the introduction of the HAT-CN/m-MTDATA OHJ has created more movable charges, which highlights the charge generation process.

The diffusion model based equation of heterojunctions has a similar form as the Shockley equation:[48]

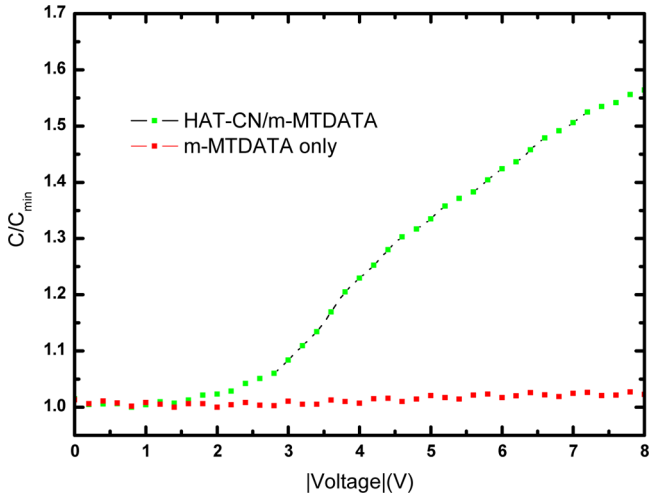

Figure 4. $C-V$ measurements of ITO and LiF(100 nm) with 20 wt % MoO_3; TAPC (50 nm) and X with 3 wt % Cs; and BPhen (50 nm), LiF(100 nm), and Al (100 nm). X is m-MTDATA (15 nm) and HAT-CN (15 nm) or m-MTDATA (15 nm) only. The voltage is also the reverse bias as above, and the tested frequency is 50 Hz.

$$J = I_0\left[\exp\left(\frac{eV}{nKT}\right) - 1\right] \quad (1)$$

where I_0 is a constant; n is the ideal factor of the junction; K is the Boltzmann constant; and T is temperature. The logarithm $J-V$ plot of the Shockley equation would give a linear relationship under a forward bias. In Figure 5, the $J-V$ curve of device D (with only m-MTDATA) shows a typical p−n junction feature, displaying a clear linear region in the single logarithm plot. The slope of the linear region corresponds to n = 2, indicating that recombination is the dominate process in that region.[49] However, this behavior is not the case in device C (with m-MTDATA/HAT-CN heterojunction); Device C shows a highly symmetric $J-V$ curve and no clear linear region. Therefore, the diffusion process cannot be described by the Shockley equation. In fact, the forward current of device C could be fitted by a charge tunneling model, as shown is Figure 5a. This behavior is similar to the reverse current of the device that will be discussed later. The formation of an accumulation heterojunction has caused a fundamental difference between device C and device D. To investigate the charge generation process of the CGL further, we tested the reverse bias $J-V$ characteristics of device C under several temperatures. The Shockley equation predicts a temperature dependence of $\ln(J) \sim 1/KT$, but the results deviate far from this prediction (see in Figure 5b, inset). Instead, the results shows a relation of $\ln(J) \sim T$ (Figure 5b), which can be found in several inorganic heterojunctions such as nGe-pGaAs and nGaSb-pGaAs.[50] Those heterojunctions have been shown to operate through a tunneling mechanism under a reverse bias.[51] Therefore, we propose that the charge generation process of the m-MTDATA/HAT-CN OHJ also operates through charge tunneling.

The tunneling equation for heterojunctions under reverse bias proposed by Riben et al. can fit our results:[52]

$$J_r = G_0 V_a \exp[-U(V_d + V_a)^{-1/2}] \quad (2)$$

where J_r is the reverse current density, G_0 is a constant determined by the nature of the material, U is a linear variable

DOI: 10.1021/acsphotonics.5b00010
ACS Photonics 2015, 2, 271−279

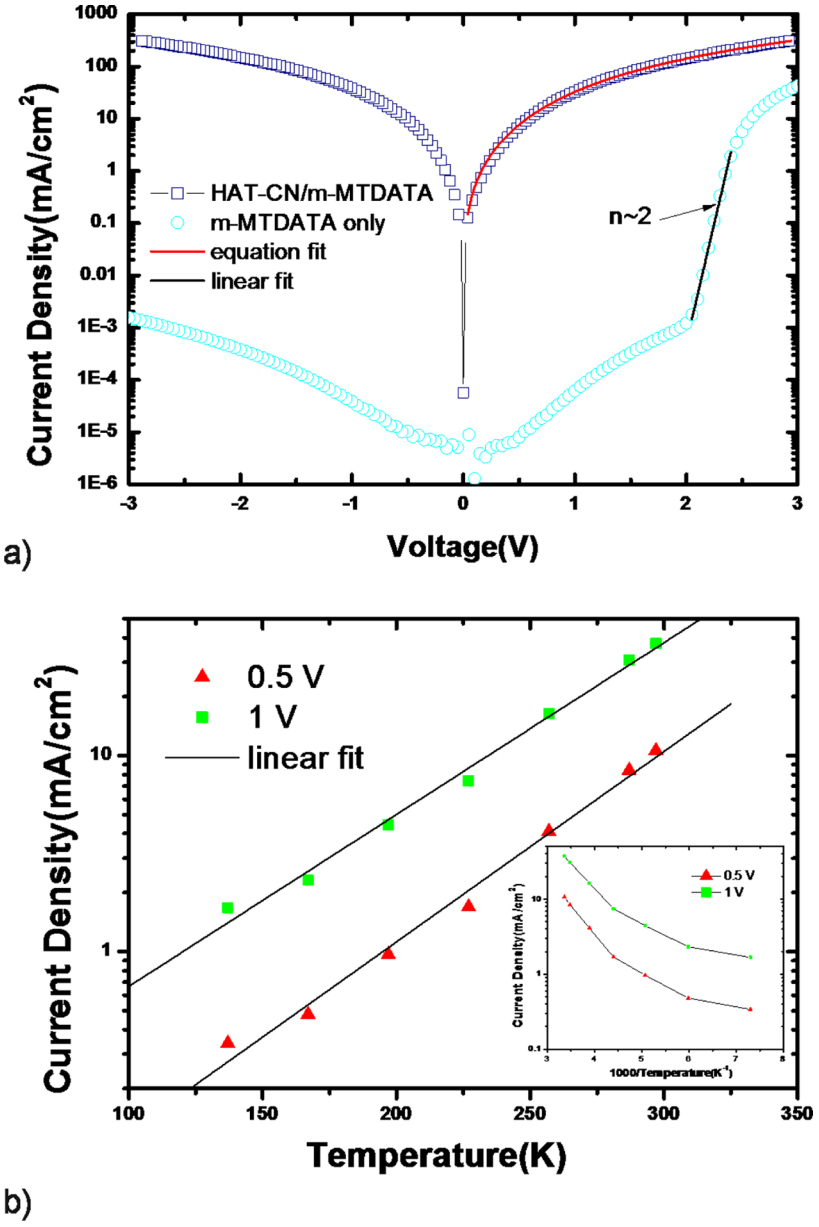

Figure 5. (a) Single logarithmic $J-V$ plot of devices A and B. (b) Temperature−current density dependence of device A under fixed voltages of 0.5 and 1 V. The inset displays a plot in (1000/K)-current density relation.

of temperature, V_d is the built-in potential, and V_a is the applied reverse voltage (written as a positive value). The equation is initially developed from the Zener tunneling equation to describe the electron tunneling from the valence band of the p-type semiconductor to the conduct band of the n-type semiconductor in staggered gap type heterojunctions. A double logarithm $J-V$ plot of device C under various temperatures is shown in Figure 6. This plot can be divided into two regions. For small voltages (~0.1 V), all curves have an identical slope of approximately 1, indicating an ideal ohmic contact and transportation which can contribute to the leakage current under small biases. For higher voltages, the curves show a power law relation and can be fitted by eq 2 at various temperatures, from 137 to 297 K. The fit further determines that the working principle of a m-MTDATA/HAT-CN CGL is Zener tunneling. The Zener tunneling explanation has also been reported by other studies to elaborate on the reverse breakdown behavior of organic semiconductors under relatively large voltages, which is distinct from our situation.[53,54] The $J-V$ properties of the m-MTDATA/HAT-CN OHJ should be explained by a charge tunneling model rather than the Shockley equation. A schematic diagram is shown in Figure 7. The band bending is depicted according to the charge accumulating property at equilibrium. When under a certain bias, the electron in the HOMO of m-MTDATA would tunnel into the LUMO of HAT-CN, thus, generating an electron in the LUMO of HAT-CN and producing a hole in the HOMO of m-MTDATA. The generated holes and electrons are then transported and injected into the adjacent layer under the influence of an electric field.

CONCLUSIONS

In conclusion, based on the experimental data and theoretical analysis presented above, we propose that the m-MTDATA/HAT OHJ operates through charge tunneling. We propose a

DOI: 10.1021/acsphotonics.5b00010
ACS Photonics 2015, 2, 271−279

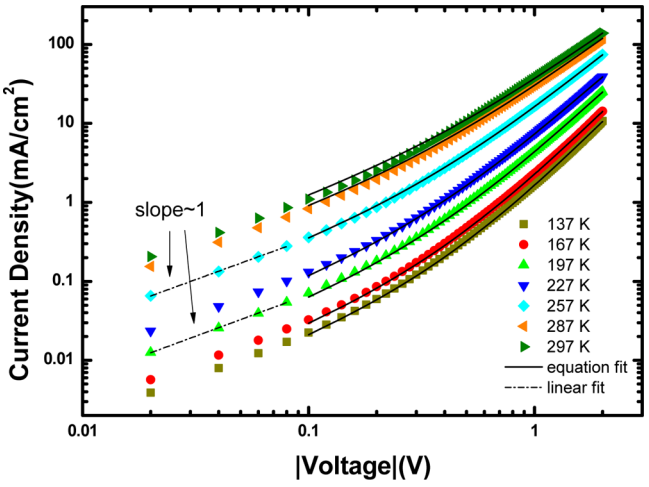

Figure 6. *J*–*V* plot of device C and the fitting curves at various temperatures; the reverse voltages are absolute values.

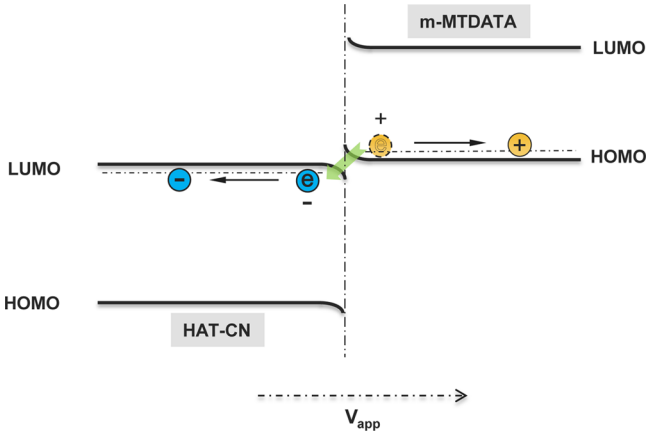

Figure 7. Schematic diagram of the charge generation process of a m-MTDATA/HAT-CN OHJ.

Zener tunneling model to represent the working mechanism of a m-MTDATA/HAT OHJ operating as a CGL, providing a new understanding of the charge generation process. Additionally, the compact tunneling equation provided for data fitting should be suitable for a series of OHJs composed in an identical manner, thus, facilitating future theoretical and experimental studies. Additionally, a green phosphorescent tandem OLED employing m-MTDATA/HAT-CN OHJ as the CGL is fabricated. After careful optimization, the tandem device achieved high current and power efficiencies and a high external quantum efficiency. We attribute the improvement to a combined effect of a better charge balance, reduced surface-plasmon loss, less electrical field induced quenching and the efficient charge generation of the m-MTDATA/HAT-CN OHJ. The voltage drop on the OHJ is small because of the charge tunneling nature, high conductivity, and large charge injection of the device.

EXPERIMENTAL SECTION

Device Fabrication. The glass substrates are sputtered with a 180 nm thick layer of patterned ITO with a sheet resistance of 10 Ω per square. The ITO surface was cleaned in an ultrasonic solvent bath and then dried at 120 °C. The ITO surface was then treated with UV ozone for 15 min before being loaded into an evaporator. All layers were grown in succession by thermal evaporation without breaking vacuum (~5 × 10−4 Pa). In the deposition of the doping layers, the deposition rates of both the host and guest were controlled with their corresponding independent quartz crystal oscillators. The evaporation rates were monitored by a frequency counter and calibrated by a Dektak 6 M profiler (Veeco). The overlap between the ITO and Al electrodes was 4 × 4 mm for the active emissive area of the devices.

Device Characterization. Current–voltage–brightness characteristics were measured using a Keithley source measurement unit (Keithley 2400 and Keithley 2000) with a calibrated silicon photodiode. The EL spectra were measured by a Spectrascan PR650 spectrophotometer. EQEs were calculated from the luminance, current density, and EL spectrum, assuming a Lambertian distribution. All measurements were performed in an ambient atmosphere. For the low-temperature *J*–*V* measurements, an Oxford Instrument Optistat DN-V cryostat system was used. Temperatures were measured within ±0.1 K by an Oxford Instrument ITC601 temperature controller.

AUTHOR INFORMATION

Corresponding Author

*E-mail: mdg1014@ciac.ac.cn.

Notes

The authors declare no competing financial interest.

ACKNOWLEDGMENTS

The authors gratefully acknowledge the National Natural Science Foundation of China (51333007, 50973104), Ministry of Science and Technology of China (973 Program No. 2013CB834805), Foundation of the Jilin Research Council (2012ZDGG001, 20130206003GX, 201105028), and Chinese Academy of Sciences (KGZD-EW-303-3) for their support of this research.

REFERENCES

(1) Murawski, C.; Leo, K.; Gather, M. C. Efficiency roll-off in organic light-emitting diodes. *Adv. Mater.* **2013**, *25*, 6801–27.

(2) Farinola, G. M.; Ragni, R. Electroluminescent materials for white organic light emitting diodes. *Chem. Soc. Rev.* **2011**, *40*, 3467–82.

(3) Wang, Q.; Ma, D. Management of charges and excitons for high-performance white organic light-emitting diodes. *Chem. Soc. Rev.* **2010**, *39*, 2387–98.

(4) Xiao, L.; Chen, Z.; Qu, B.; Luo, J.; Kong, S.; Gong, Q.; Kido, J. Recent progresses on materials for electrophosphorescent organic light-emitting devices. *Adv. Mater.* **2011**, *23*, 926–52.

(5) Sun, N.; Wang, Q.; Zhao, Y.; Chen, Y.; Yang, D.; Zhao, F.; Chen, J.; Ma, D. High-performance hybrid white organic light-emitting devices without interlayer between fluorescent and phosphorescent emissive regions. *Adv. Mater.* **2014**, *26*, 1617–21.

(6) Sasabe, H.; Takamatsu, J.; Motoyama, T.; Watanabe, S.; Wagenblast, G.; Langer, N.; Molt, O.; Fuchs, E.; Lennartz, C.; Kido, J. High-efficiency blue and white organic light-emitting devices incorporating a blue iridium carbene complex. *Adv. Mater.* **2010**, *22*, 5003–7.

(7) Wang, Z. B.; Helander, M. G.; Qiu, J.; Puzzo, D. P.; Greiner, M. T.; Hudson, Z. M.; Wang, S.; Liu, Z. W.; Lu, Z. H. Unlocking the full potential of organic light-emitting diodes on flexible plastic. *Nat. Photonics* **2011**, *5*, 753–757.

(8) Reineke, S.; Lindner, F.; Schwartz, G.; Seidler, N.; Walzer, K.; Lussem, B.; Leo, K. White organic light-emitting diodes with fluorescent tube efficiency. *Nature* **2009**, *459*, 234–8.

DOI: 10.1021/acsphotonics.5b00010
ACS Photonics 2015, 2, 271–279

(9) Uoyama, H.; Goushi, K.; Shizu, K.; Nomura, H.; Adachi, C. Highly efficient organic light-emitting diodes from delayed fluorescence. *Nature* **2012**, *492*, 234−8.
(10) Helander, M. G.; Wang, Z. B.; Qiu, J.; Greiner, M. T.; Puzzo, D. P.; Liu, Z. W.; Lu, Z. H. Chlorinated indium tin oxide electrodes with high work function for organic device compatibility. *Science* **2011**, *332*, 944−7.
(11) Liao, L. S.; Klubek, K. P.; Tang, C. W. High-efficiency tandem organic light-emitting diodes. *Appl. Phys. Lett.* **2004**, *84*, 167−169.
(12) Birnstock, J.; He, G. F.; Murano, S.; Wemer, A.; Zeika, O. Distinguished paper: White stacked OLED with 35 lm/W and 100000 h lifetime at 1000 cd/m(2) for display and lighting applications. *2008 Sid International Symposium, Digest of Technical Papers*; SID: Campbell, CA, 2008; Vol *XXXIX*, Books I−III, pp822−825
(13) Liao, L. S.; Slusarek, W. K.; Hatwar, T. K.; Ricks, M. L.; Comfort, D. L. Tandem organic light-emitting diode using hexaazatriphenylene hexacarbonitrile in the intermediate connector. *Adv. Mater.* **2008**, *20*, 324−329.
(14) Chen, Y. H.; Chen, J. S.; Ma, D. G.; Yan, D. H.; Wang, L. X. Tandem white phosphorescent organic light-emitting diodes based on interface-modified C-60/pentacene organic heterojunction as charge generation layer. *Appl. Phys. Lett.* **2011**, *99*, 103304.
(15) Chiba, T.; Pu, Y. J.; Miyazaki, R.; Nakayama, K.; Sasabe, H.; Kido, J. Ultra-high efficiency by multiple emission from stacked organic light-emitting devices. *Org. Electron.* **2011**, *12*, 710−715.
(16) Kanno, H.; Holmes, R. J.; Sun, Y.; Kena-Cohen, S.; Forrest, S. R. White stacked electrophosphorescent organic light-emitting devices employing MoO3 as a charge-generation layer. *Adv. Mater.* **2006**, *18*, 339−342.
(17) Liao, L. S.; Klubek, K. P. Power efficiency improvement in a tandem organic light-emitting diode. *Appl. Phys. Lett.* **2008**, *92*, 223311.
(18) Tang, J. X.; Fung, M. K.; Lee, C. S.; Lee, S. T. Interface studies of intermediate connectors and their roles in tandem OLEDs. *J. Mater. Chem.* **2010**, *20*, 2539−2548.
(19) Baldo, M. A.; O'Brien, D. F.; You, Y.; Shoustikov, A.; Sibley, S.; Thompson, M. E.; Forrest, S. R. Highly efficient phosphorescent emission from organic electroluminescent devices. *Nature* **1998**, *395*, 151−154.
(20) Baldo, M. A.; Adachi, C.; Forrest, S. R. Transient analysis of organic electrophosphorescence. II. Transient analysis of triplet-triplet annihilation. *Phys. Rev. B* **2000**, *62*, 10967−10977.
(21) Hamwi, S.; Meyer, J.; Kroger, M.; Winkler, T.; Witte, M.; Riedl, T.; Kahn, A.; Kowalsky, W. The role of transition metal oxides in charge-generation layers for stacked organic light-emitting diodes. *Adv. Funct. Mater.* **2010**, *20*, 1762−1766.
(22) Deng, Y.-H.; Ou, Q.-D.; Wang, Q.-K.; Wei, H.-X.; Li, Y.-Q.; Lee, S.-T.; Tang, J.-X. The role of charge generation layers in the operational stability of tandem organic light-emitting diodes. *J. Mater. Chem. C* **2014**, *2*, 1982−1989.
(23) Su, S. J.; Gonmori, E.; Sasabe, H.; Kido, J. Highly efficient organic blue-and white-light-emitting devices having a carrier- and exciton-confining structure for reduced efficiency roll-off. *Adv. Mater.* **2008**, *20*, 4189−4194.
(24) Walzer, K.; Maennig, B.; Pfeiffer, M.; Leo, K. Highly efficient organic devices based on electrically doped transport layers. *Chem. Rev.* **2007**, *107*, 1233−71.
(25) Tao, Y.; Wang, Q.; Yang, C.; Zhong, C.; Qin, J.; Ma, D. Multifunctional triphenylamine/oxadiazole hybrid as host and exciton-blocking material: high efficiency green phosphorescent OLEDs using easily available and common materials. *Adv. Funct. Mater.* **2010**, *20*, 2923−2929.
(26) Liu, H. H.; Yan, F.; Wang, H.; Miao, Y. Q.; Du, X. G.; Jing, S.; Gao, Z. X.; Chen, L. Q.; Hao, Y. Y.; Xu, B. S. Efficient tandem organic light-emitting device based on photovoltaic-type connector with positive cycle. *Appl. Phys. Lett.* **2013**, *102*, 013304.
(27) Rao, M. V. M; Huang, T. S.; Su, Y. K.; Huang, Y. T. Fullerene and pentacene as a pure organic connecting layer in tandem organic light emitting devices. *J. Electrochem. Soc.* **2010**, *157*, H69−H71.
(28) Chen, Y. H.; Tian, H. K.; Geng, Y. H.; Chen, J. S.; Ma, D. G.; Yan, D. H.; Wang, L. X. Organic heterojunctions as a charge generation layer in tandem organic light-emitting diodes: the effect of interfacial energy level and charge carrier mobility. *J. Mater. Chem.* **2011**, *21*, 15332−15336.
(29) Chen, Y. H.; Wang, Q.; Chen, J. S.; Ma, D. G.; Yan, D. H.; Wang, L. X. Organic semiconductor heterojunction as charge generation layer in tandem organic light-emitting diodes for high power efficiency. *Org. Electron.* **2012**, *13*, 1121−1128.
(30) Chen, Y. H.; Chen, J. S.; Ma, D. G.; Yan, D. H.; Wang, L. X.; Zhu, F. R. High power efficiency tandem organic light-emitting diodes based on bulk heterojunction organic bipolar charge generation layer. *Appl. Phys. Lett.* **2011**, *98*, 243309.
(31) Chen, Y. H.; Chen, J. S.; Ma, D. G.; Yan, D. H.; Wang, L. X. Effect of organic bulk heterojunction as charge generation layer on the performance of tandem organic light-emitting diodes. *J. Appl. Phys.* **2011**, *110*, 074504.
(32) Hoppe, H.; Sariciftci, N. S. Organic solar cells: An overview. *J. Mater. Res.* **2011**, *19*, 1924−1945.
(33) Sullivan, P.; Heutz, S.; Schultes, S. M.; Jones, T. S. Influence of codeposition on the performance of CuPc−C[sub 60] heterojunction photovoltaic devices. *Appl. Phys. Lett.* **2004**, *84*, 1210.
(34) Lai, S. L.; Chan, M. Y.; Fung, M. K.; Lee, C. S.; Lee, S. T. Copper hexadecafluorophthalocyanine and copper phthalocyanine as a pure organic connecting unit in blue tandem organic light-emitting devices. *J. Appl. Phys.* **2007**, *101*, 014509.
(35) Falkenberg, C.; Olthof, S.; Rieger, R.; Baumgarten, M.; Muellen, K.; Leo, K.; Riede, M. The role of energy level matching in organic solar cells-hexaazatriphenylene hexacarbonitrile as transparent electron transport material. *Sol. Energy Mater. Sol. Cells* **2011**, *95*, 927−932.
(36) Kroger, M.; Hamwi, S.; Meyer, J.; Dobbertin, T.; Riedl, T.; Kowalsky, W.; Johannes, H.-H. Temperature-independent field-induced charge separation at doped organic/organic interfaces: Experimental modeling of electrical properties. *Phys. Rev. B* **2007**, *75*, 235321.
(37) Seo, J. H.; Han, N. S.; Shim, H. S.; Park, S. M.; Kwon, J. H.; Song, J. K. Triplet state and phosphorescence of hole-transport layer and its triplet exciton confinement. *Chem. Phys. Lett.* **2010**, *499*, 226−230.
(38) Wünsche, J.; Reineke, S.; Lüssem, B.; Leo, K. Measurement of triplet exciton diffusion in organic light-emitting diodes. *Phys. Rev. B* **2010**, *81*, 245201.
(39) Tsuzuki, T.; Tokito, S. Highly efficient and low-voltage phosphorescent organic light-emitting diodes using an iridium complex as the host material. *Adv. Mater.* **2007**, *19*, 276−280.
(40) Olthof, S.; Meerheim, R.; Schober, M.; Leo, K. Energy level alignment at the interfaces in a multilayer organic light-emitting diode structure. *Phys. Rev. B* **2009**, *79*, 245308.
(41) Meyer, J.; Hamwi, S.; Kroger, M.; Kowalsky, W.; Riedl, T.; Kahn, A. Transition metal oxides for organic electronics: energetics, device physics and applications. *Adv. Mater.* **2012**, *24*, 5408−27.
(42) Cho, T. Y.; Lin, C. L.; Wu, C. C. Microcavity two-unit tandem organic light-emitting devices having a high efficiency. *Appl. Phys. Lett.* **2006**, *88*, 111106.
(43) Yan, D.; Wang, H.; Du, B. *Introduction to Organic Semiconductor Heterojunctions*; John Wiley & Sons: New York, 2010; pp 91−93.
(44) Lee, S.; Lee, J. H.; Lee, J. H.; Kim, J. J. The mechanism of charge generation in charge-generation units composed of p-doped hole-transporting layer/HATCN/n-doped electron-transporting layers. *Adv. Funct. Mater.* **2012**, *22*, 855−860.
(45) Meerheim, R.; Lussem, B.; Leo, K. Efficiency and stability of p-i-n type organic light emitting diodes for display and lighting applications. *Proc. IEEE* **2009**, *97*, 1606−1626.
(46) Yook, K. S.; Jeon, S. O.; Min, S.-Y.; Lee, J. Y.; Yang, H.-J.; Noh, T.; Kang, S.-K.; Lee, T.-W. Highly efficient p-i-n and tandem organic light-emitting devices using an air-stable and low-temperature-evaporable metal azide as an n-dopant. *Adv. Funct. Mater.* **2010**, *20*, 1797−1802.

DOI: 10.1021/acsphotonics.5b00010
ACS Photonics 2015, 2, 271−279

(47) Yang, J.-P.; Xiao, Y.; Deng, Y.-H.; Duhm, S.; Ueno, N.; Lee, S.-T.; Li, Y.-Q.; Tang, J.-X. Electric-field-assisted charge generation and separation process in transition metal oxide-based interconnectors for tandem organic light-emitting diodes. *Adv. Funct. Mater.* **2012**, *22*, 600−608.
(48) Anderson, R. L. Experiments on Ge-GaAs heterojunctions. *Solid-State Electron.* **1962**, *5*, 341−351.
(49) Sah, C. T.; Noyce, R. N.; Shockley, W. Carrier generation and recombination in P-N junctions and P-N junction characteristics. *Proc. Inst. Radio Eng.* **1957**, *45*, 1228−1243.
(50) Newman, P. C. Forward—Characteristics of heterojunctions. *Electron. Lett.* **1965**, *1*, 265.
(51) Riben, A. R.; Feucht, D. L. nGe·pGaAs Heterojunctions. *Solid-State Electron.* **1966**, *9*, 1055−1065.
(52) Riben, A. R.; Feucht, D. L. Electrical transport in Nge-Pgaas heterojunctions. *Int. J. Electron.* **1966**, *20*, 583−599.
(53) Kleemann, H.; Gutierrez, R.; Lindner, F.; Avdoshenko, S.; Manrique, P. D.; Lussem, B.; Cuniberti, G.; Leo, K. Organic Zener diodes: tunneling across the gap in organic semiconductor materials. *Nano Lett.* **2010**, *10*, 4929−34.
(54) Kleemann, H.; Gutierrez, R.; Avdoshenko, S.; Cuniberti, G.; Leo, K.; Luessem, B. Reverse breakdown behavior in organic pin-diodes comprising C60 and pentacene: Experiment and theory. *Org. Electron.* **2013**, *14*, 193−199.

DOI: 10.1021/acsphotonics.5b00010
ACS Photonics 2015, 2, 271−279